Jpn. J. Appl. Phys. Vol. 33 (1994) pp. 869-872
Part 1, No. 1B, January 1994

Very Long Wavelength Intersubband Infrared Hot Electron Transistor

Sarath D. GUNAPALA, John K. LIU, True L. LIN and Jin S. PARK
Center for Space Microelectronics Technology, Jet Propulsion Laboratory, California Institute of Technology, Pasadena, CA 91091, U.S.A.

(Received September 17, 1993; accepted for publication November 20, 1993)

We have demonstrated the first very long wavelength (16 μm) infrared hot electron transistor (IHET). This device utilizes a bound to continuum GaAs/$Al_xGa_{1-x}As$ ($x=0.11$) quantum well infrared photodetector (QWIP) as a photosensitive emitter, a wide quantum well as a base, and a thick $Al_xGa_{1-x}As$ ($x=0.11$) barrier between the base and the collector as an energy discriminating filter. This energy filter blocks the lower energy tunneled electrons, which drain through the base while higher energy photo electrons pass to the collector. Therefore, the detectivity of the device at the collector is much higher than the detectivity at the emitter.

KEYWORDS: quantum well, hot electron, intersubband, infrared detectors and long wavelength

1. Introduction

Very long wavelength infrared (IR) detectors and imaging systems are required in many space applications such as the atmospheric IR sounder (AIRS) and the tropospheric emission spectrometer (TES) instruments which will be used in NASA's earth observation system (EOS). The wavelength of the IR radiation required in these applications range from 3.7 to 15.4 μm. These space applications have placed stringent requirements on the performance of the IR detectors and arrays including high detectivity, low dark current, uniformity and radiation hardness. This paper will present the study and development of a low dark current very long wavelength intersubband IR hot electron transistor (IHET).

There has been a lot of interest recently in the detection of very long wavelength ($\lambda=12$-16 μm) infrared radiation using multiple quantum wells, due to the fact that these quantum well IR photodetectors[1-13] (QWIPs) and IHETs[8,14-16] can be fabricated using the mature III-V materials growth and processing technologies. This superior materials control results in high uniformity and thus allows fabrication of large staring arrays ($\lambda=8$-12 μm) with excellent imaging performance.[17-19] One of the problems associated with the very long wavelength QWIPs is the higher dark current which adversely affects detector performance. By analyzing the dark current of shallow quantum wells we have realized that the total tunneling current (sequential tunneling + thermionic assisted tunneling) is significantly higher than the thermionic dark current (Fig. 1). The conduction electrons carrying these two tunneling current components are lower in energy than the photoelectrons.[8] Therefore, a 16 μm GaAs/$Al_xGa_{1-x}As$ IHET which can effectively filter out sequential tunneling and thermionic assisted tunneling currents was fabricated.

2. Dark Current

In this section the dark current of a single quantum well, which has intersubband absorption peak at 16 μm will be analyzed. First effective number of electrons[11,20] $n(V)$ which are thermally excited into the continuum transport states, as a function of bias voltage V were calculated.

$$n(V)=\left(\frac{m^*}{\pi\hbar^2 L_p}\right)\int_{E_0}^{\infty} f(E)T(E,\,V)\,dE.$$

The first factor containing the effective mass m^* represents the average three dimensional density of states. Where L_p is the superlattice period, $f(E)$ is the Fermi factor $f(E)=[1+\exp(E-E_0-E_F)/KT]^{-1}$, E_0 is the bound state energy, E_F is the two-dimensional Fermi energy, E is the energy of the electron, and $T(E,\,V)$ is the tunneling current transmission factor. This tunneling transmission factor obtained by applying WKB approximation to a biased quantum well is:

$$T(E)=(4\sqrt{E}\sqrt{(V_0-E)}/V_0)e^{-2\tau}$$

where $\tau=(2L\sqrt{2m^*}/3\hbar\Delta V)(V_0-E)^{3/2}$, V_0 is the barrier height, ΔV is the bias voltage per superlattice period, and L is the barrier width. The number of electrons, given by $n(V)$ accounts for thermionic emission above the barrier height when $E>V_0$ and thermionic assisted

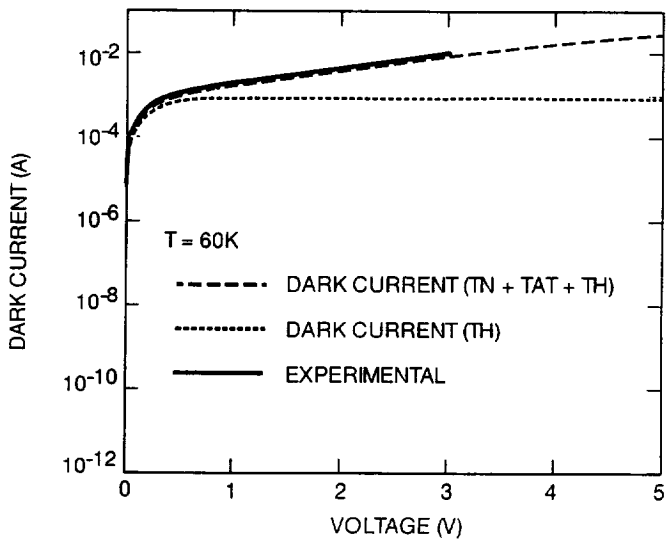

Fig. 1. Theoretical and experimental (solid) dark current-voltage curves at $T=60$ K. Dotted curve shows the dark current (theoretical) due to thermionic emission only. Dashed curve shows the total dark current (thermionic + tunneling + thermionic assisted) versus bias voltage.

tunneling and tunneling when $E < V_0$. Then the bias-dependent dark current $I_d(V)$ was calculated, using $I_d(V) = eAn(V)v(V)$, *where* $v(V)$ is the average transport velocity, A is the device area, and e is the electronic charge. The average transport velocity was calculated using $v(V) = \mu F[1 + (\mu F/v_s)^2]^{-1/2}$, where μ is the mobility, F is the electric field, and v_s is the saturated drift velocity. In order to obtain $T = 60$ K bias-dependent dark current $\mu = 1200$ cm^2/Vs, and $v_s = 5.5 \times 10^6$ cm/s was used. Figure 1 shows the $T = 60$ K dark current due to thermionic emission, total dark current (thermionic + thermionic assisted tunneling + tunneling), and experimental dark current of a QWIP sample which has wavelength cutoff $\lambda_c = 17.8$ μm. According to the calculations tunneling through the barriers dominate the dark current at temperatures below 30 K, at temperatures between 40–60 K thermionic assisted tunneling might become important, and at temperatures above 60 K thermionic emission into the continuum transport states dominate the dark current.

3. Experiment

As shown in Fig. 2 the device structure consisted of a multi-quantum well region of 50 periods of 500 Å undoped $Al_{0.11}Ga_{0.89}As$ barrier and 65 Å doped GaAs well. The quantum wells were doped to $n = 5 \times 10^{17}$ cm^{-3}, and sandwiched between a heavily doped ($n = 1 \times 10^{18}$ cm^{-3}) 1 μm GaAs contact layer at the bottom as the emitter contact and a doped ($n = 3 \times 10^{17}$ cm^{-3}) 500 Å GaAs layer on the top as the base contact. On top of the base a 2000 Å undoped $Al_{0.11}Ga_{0.89}As$ layer and a doped ($n = 3 \times 10^{17}$ cm^{-3}) 0.5 μm GaAs layer were grown. The 2000 Å undoped $Al_{0.11}Ga_{0.89}As$ As layer acted as a discriminator between the tunnel-electrons and photoelectrons, and the top 0.5 μm GaAs layer served as the collector. This device structure was grown on a semi-insulating GaAs substrate using molecular beam epitaxy. The inset of the Fig. 2 shows the diagram of the device. QWIP operation can be obtained between the emitter and the base and all the terminals (three) are required for the IHET operation. The IHET currents were measured at the collector (low energy tunneled electrons drain through the base).

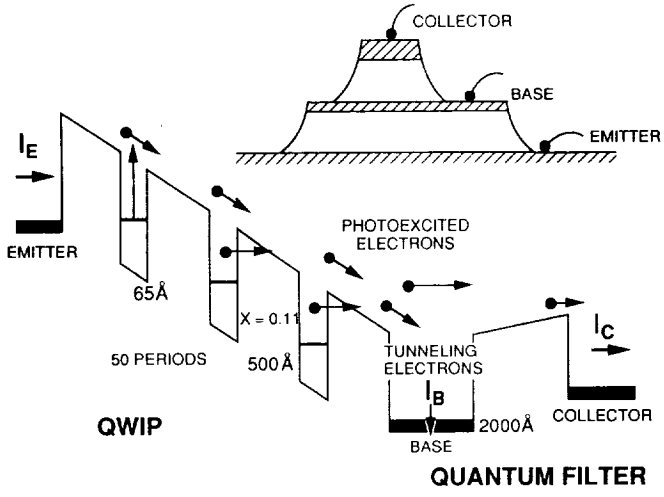

Fig. 2. Conduction-band diagram of a infrared hot electron transistor, which utilizes bound to continuum intersubband transition. The inset shows the diagram of IHET.

The intersubband absorption was measured on a 45° polished multipass waveguide[21] as shown in the inset of Fig. 3. As shown in the Fig. 3 the $T = 300$ K absorption coefficient spectra α_p has a peak infrared absorption coefficient $\alpha_p = 534$ cm^{-1} at $\lambda_p = 17.1$ μm with absorption half heights at 14.2 and 18 μm (i.e., a full width at half maximum of $\Delta\lambda = 3.8$ μm). At low temperature the half width narrows and the peak absorption coefficient increases[22,23] by a factor of 1.3 so that $\alpha_p = 694$ cm^{-1} at $T = 60$ K corresponding to an unpolarized quantum efficiency $\eta = (1 - e^{-2\alpha l})/2 = 16.5\%$.

To facilitate the application of bias to the quantum well structure, the following processing steps were carried out. First arrays of 200×200 μm^2 square collectors were chemically etched. In the next processing step the 6.25×10^{-4} cm^2 QWIP mesas which overlap with collector mesas were etched (inset of Fig. 2). Finally, Au/Ge ohmic contacts were evaporated onto the emitter, base and collector contact layers. The emitter and collector dark currents versus base-collector bias voltage are shown in Fig. 4. This figure also shows the lower energy dark current filtration capability of the quantum filter. The dark current transfer ratio ($\alpha_{dark} = I_{Collector(dark)}/I_{Emitter(dark)}$) is 7.2×10^{-5} at operating base-collector bias voltage $V_{CB} = -42$ mV.

These 200×200 μm^2 square detectors were back illuminated through a 45° polished facet as described in detail previously[1] and responsivity spectra were measured with a tunable source consisting of a 1000 K black-

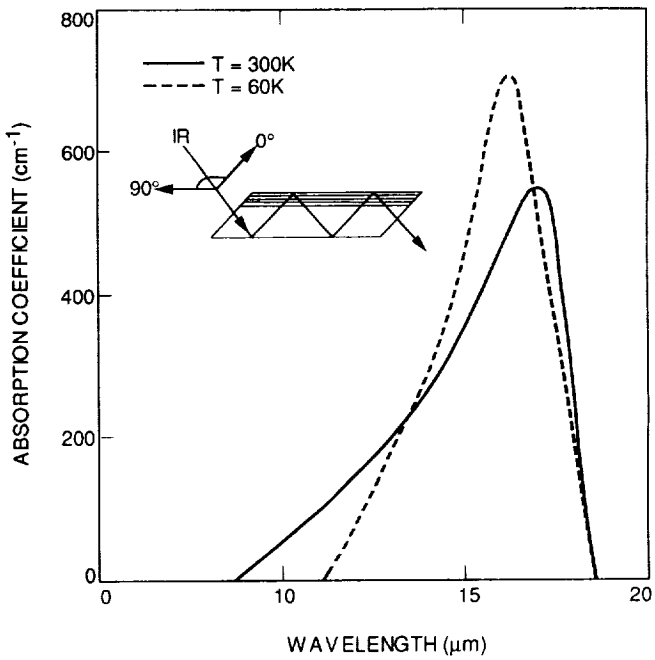

Fig. 3. Absorption coefficient spectra $\alpha(\lambda)$ of the long wavelength quantum well infrared detector. The solid line shows the absorption coefficient at $T = 300$ K and the dashed line shows the absorption curve at $T = 60$ K. This absorption spectra was measured at room temperature using a 45° multipass waveguide geometry as shown in the inset.

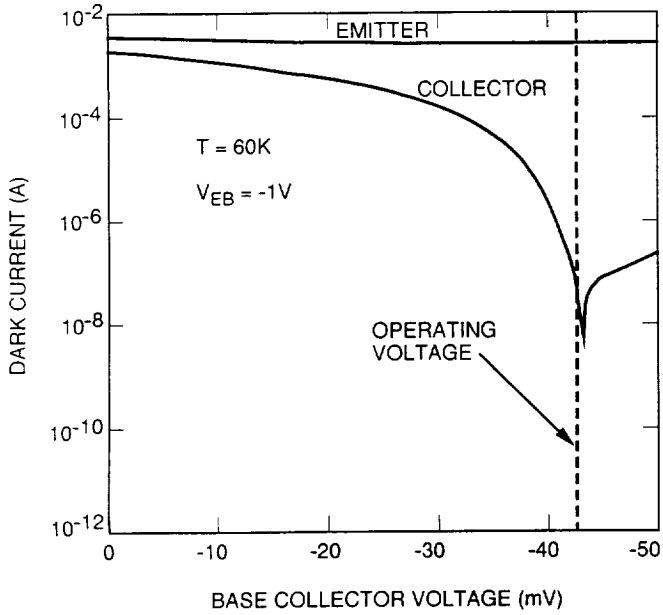

Fig. 4. IHET emitter and collector dark currents versus base-collector voltage at $T=60$ K. Emitter bias was kept at -1 V relative to the base potential. This figure also shows the lower energy dark current filtration capability of the quantum filter.

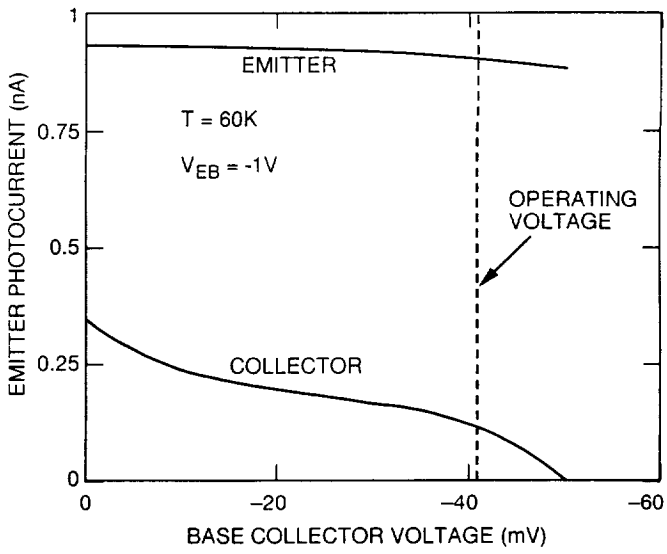

Fig. 6. IHET emitter and collector photo currents Vs base-collector voltage at $T=60$ K. Emitter was kept at -1 V bias relative to the base potential.

body and a grating monochromator. The emitter and collector responsivity spectrum measured at $T=60$ K is shown in Fig. 5. The values of the peak wavelength λ_p, cutoff wavelength λ_c and the spectral width $(\Delta\lambda/\lambda)$ (full width at half maximum) are 16.3 μm, 17.3 μm and 20% respectively. The absolute responsivity was measured by two different methods, comparison with calibrated pyroelectric detector and, using a calibrated blackbody source. The peak responsivity Rp of the detector was 400 mA/W, while the peak responsivity and the shape of the spectra were independent of the measuring technique as expected. Fig. 6 shows the IHET emitter and collector photo currents versus base-collector voltage at $T=60$ K. The emitter was kept at -1 V bias relative to the base potential. Due to the hot electron relaxation in the wide base region, the photo current at collector is smaller relative to the emitter photo current. Photo current transfer ratio ($\alpha_{photo}=I_{Collector(photo)}/I_{Emitter(photo)}$) is 1.2×10^{-1} at $V_{CB}=-42$ mV. It is worth noticing that α_{dark} is more than three orders of magnitude smaller than α_{photo}. This clearly indicates that the dark current of IHET is four orders of magnitude smaller than the dark current of QWIP while the photo current is reduced by an order of magnitude only. This four orders of magnitude reduction in dark current reduces the noise current by two orders of magnitude (and hence higher detectivity).

4. Results

The optical gain g of the detector determined from $R=(e/h\nu)\eta g$ is given by $g=0.2$. The noise current[24] in

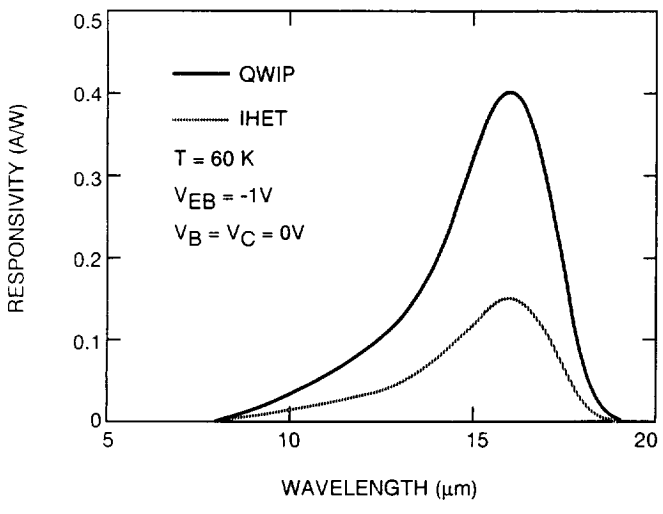

Fig. 5. The emitter (QWIP) and collector (IHET) responsivity spectrums at $T=60$ K. Emitter was kept at -1 V bias relative to the base and collector.

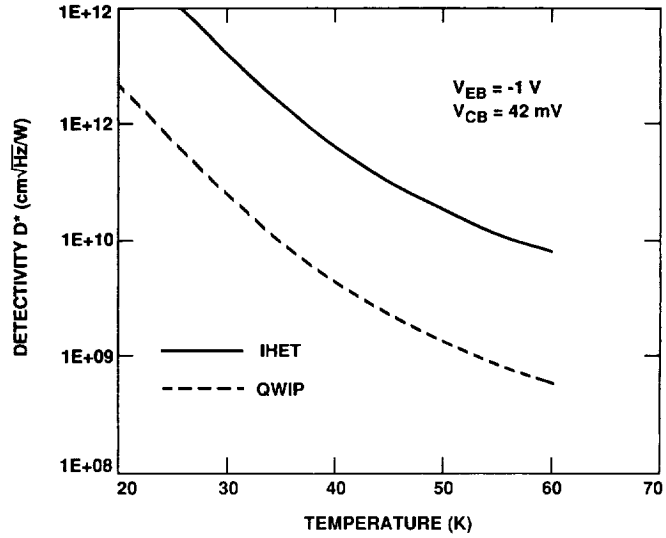

Fig. 7. Peak detectivity of QWIP and IHET having a cut-off wavelength of $=17.3$ μm as a function of temperature T.

was calculated using $i_n=\sqrt{4eI_d g\Delta f}$, where Δf is the bandwidth. The calculated noise current of the detector is $i_n=17$ pA at $T=60$ K. The peak D^* can now be calculated from $D^*=R\sqrt{A\Delta f}/i_n$. The calculated D^* between the emitter and the base (QWIP) at $V_{EB}=-1$ V, $V_{CB}=-42$ mV and $T=60$ K is 5.8×10^8 cm $\sqrt{\text{Hz}}$/W. The detectivity D^* at the collector (IHET) is determined[5] from $D^*(\text{IHET})=(\alpha_{photo}/\sqrt{\alpha_{dark}})\ D^*$ (QWIP) is given by D^* (IHET) $=8.2\times10^9$ cm $\sqrt{\text{Hz}}$/W at $T=60$ K. As shown in Fig. 7 detectivity D^* increases dramatically with decreasing temperature reaching $D^*=1\times10^{12}$ cm $\sqrt{\text{Hz}}$/W at $T=25$ K and is even larger at lower temperatures. In contrast, detectivity D^* of HgCdTe detectors are about 1×10^{11} cm $\sqrt{\text{Hz}}$/W at $T=60$ K at similar wavelengths and does not increase as the temperature is lowered.

5. Conclusion

In conclusion, we have demonstrated the first very long wavelength ($\lambda_c=17.3\,\mu$m) IHET. This device clearly shows the dark current filtration capability of the energy filter. Therefore, the D^* of IHET is much higher than the D^* of two terminal multi quantum well detector.

Acknowledgments

We are grateful to K. K. Choi of the Army Research Laboratory and K. M. S. V. Bandara and B. F. Levine of the AT & T Bell Laboratories for many useful discussions and C. A. Kukkonen, V. Sarohia, S. Khanna, K. M. Koliwad, B. A. Wilson, and P. J. Grunthaner of the Jet Propulsion Laboratory for encouragement and support of this work. The research described in this paper was performed by the Center for space Microelectronics Technology, Jet Propulsion Laboratory, California Institute of Technology, and was jointly sponsored by the Ballistic Missile Defense Organization/Innovative Science and Technology Office, and the National Aeronautics and Space Administration, Office of Advanced Concepts and Technology.

1) B. F. Levine, C. G. Bethea, G. Hasnain, J. Walker and R. J. Malik: Appl. Phys. Lett. **53** (1988) 296.
2) B. F. Levine: *Proc. NATO Advanced Research Workshop on Intersubband Transitions in Quantum Wells, Cargese, 1991*, eds. E. Rosencher, B. Vinter and B. F. Levine (Plenum, London, 1992).
3) J. Y. Andersson and L. Lundqvist: Appl. Phys. Lett. **59** (1991) 857.
4) S. D. Gunapala, B. F. Levine, D. Ritter, R. A. Hamm and M. B. Panish: Appl. Phys. Lett. **58** (1991) 2024.
5) S. D. Gunapala, B. F. Levine, D. Ritter, R. A. Hamm and M. B. Panish: Appl. Phys. Lett. **60** (1992) 636.
6) B. K. Janousek, M. J. Daugherty, W. L. Bloss, M. L. Rosenbluth, M. J. O'Loughlin, H. Kanter, F. J. De Luccia and L. E. Perry: J. Appl. Phys. **67** (1990) 7608.
7) S. R. Andrews and B. A. Miller: J. Appl. Phys. **70** (1991) 993.
8) K. K. Choi, M. Dutta, P. G. Newman, M. L. Saunders and G. L. Iafrate: Appl. Phys. Lett. **57** (1990) 1348.
9) L. S. Yu and S. S. Li: Appl. Phys. Lett. **59** (1991) 1332.
10) A. G. Steele, H. C. Liu, M. Buchanan and Z. R. Wasilewski: Appl. Phys. Lett. **59** (1991) 3625.
11) S. D. Gunapala, B. F. Levine, L. Pfeiffer and K. West: J. Appl. Phys. **69** (1990) 6517.
12) M. J. Kane S. Millidge, M. T. Emeny, D. Lee, D. R. P. Guy and C. R. Whitehouse: *Proc. NATO Advanced Research Workshop on Intersubband Transitions in Quantum Wells, Cargese*, 1991, eds. E. Rosencher, B. Vinter and B. F. Levine (Plenum, London, 1992).
13) C. S. Wu, C. P. Wen, R. N. Sato, M. Hu, C. W. Tu, J. Zhang, L. D. Flesner, L. Pham and P. S. Nayer: IEEE Trans. Electron Devices **39** (1992) 234.
14) K. K. Choi, M. Dutta and R. P. MoerKirk: Appl. Phys. Lett. **58** (1991) 1533.
15) K. K. Choi, M. Taysing-Lara, L. Fotiadis and W. Chang: Appl. Phys. Lett. **59** (1991) 1614.
16) K. K. Choi, L. Fotiadis, M. Taysing-Lara and W. Chang: Appl. Phys. Lett. **59** (1991) 3303.
17) B. F. Levine, C. G. Bethea, K. G. Glogovsky, J. W. Stayt and R. E. Labenguth: Semicon. Sci. Technol. **6** (1991) c114.
18) M. T. Asom *et al.*: *Proc. IRIS Specialty Group on Infrared Materials, Boulder, CO, August 12–16, 1991*, Vol. 1, p. 13.
19) L. J. Kozlowski, G. M. Williams, G. J. Sullivan, C. W. Farley, R. J. Anderson, J. K. Chen, D. T. Cheung, W. E. Tennant and R. E. DeWames: IEEE Trans. Electron Devices **38** (1991) 1124.
20) B. F. Levine, C. G. Bethea, G. Hasnain, V. O. Shen, E. Pelve, R. R. Abbott and S. J. Hsieh: Appl. Phys. Lett. **56** (1990) 851.
21) B. F. Levine, R. J. Malik, J. Walker, K. K. Choi, C. G. Bethea, D. A. Kleinman and J. M. Vandenberg: Appl. Phys. Lett. **50** (1987) 273.
22) G. Hasnain, B. F. Levine, C. G. Bethea, R. R. Abbott and S. J. Hsieh: J. Appl. Phys. **67** (1990) 4361.
23) M. O. Manasreh, F. Szmuiowicz, D. W. Fischer, K. R. Evans and C. E. Stutz: Appl. Phys. Lett. **57** (1990) 1790.
24) B. F. Levine, A. Zussman, S. D. Gunapala, M. T. Asom, J. M. Kuo and W. S. Hobson: J. Appl. Phys. **72** (1992) 4429.